Ancient subcontinental ultra-depleted mantle-derived crust and its role in Phanerozoic magmatism of Central Asian Orogenic Belt

Huichuan Liu [1, 2, *], Gongjian Tang [3], Weiming Fan[4, 5]

1 State Key Laboratory of Petroleum Resources and Prospecting, China University of Petroleum (Beijing), Beijing 102249, China

2 College of Geosciences, China University of Petroleum (Beijing), Beijing 102249, China

3 State Key Laboratory of Isotope Geochemistry, Guangzhou Institute of Geochemistry, Chinese Academy of Sciences, Guangzhou 510640, China

4 Key Laboratory of Continental Collision and Plateau Uplift, Institute of Tibetan Plateau Research, Chinese Academy of Sciences, Beijing 100101, China

5 College of Earth and Planetary Sciences, University of Chinese Academy of Sciences, Beijing 141407, China

*Corresponding author

Abstract:

Ultra-depleted mantle (UDM), characterized by Nd-Hf isotopically more depleted than mid-ocean ridge basalt, is ubiquitous beneath the oceanic crust, but no UDM has been reported underneath the continental crust. The Central Asian Orogenic Belt (CAOB) preserves large volumes of Phanerozoic granitoids with elevated $_{Nd}(t)-_{Hf}(t)$ and is regarded as the largest site of Phanerozoic crustal growth on Earth. Ancient (ca. 1.7 Ga) subcontinental UDM with extremely high $_{Nd}(t)-_{Hf}(t)$ values was identified beneath the CAOB for the first time based on finding of 1.7 Ga diorite intrusions with extremely high $_{Nd}(t)$, $_{Hf}(t)$ and ^{18}O values, and significant Nd-Hf isotope decoupling. Partial melting of 1.7 Ga subcontinental UDM produced widely distributed 1.7 Ga crust with ultrahigh $_{Nd}(t)-_{Hf}(t)$ values, and subsequent episodic remelting of this crust generated the Phanerozoic high $_{Nd}(t)-_{Hf}(t)$ granitoids in the CAOB. Phanerozoic crustal growth in accretionary orogens as exemplified by the CAOB may have been overestimated.

Keywords: Ultra-depleted mantle; Accretionary orogen; Phanerozoic crustal growth; Nd–Hf isotope decoupling; Central Asian Orogenic Belt; Crustal reworking

Plain language summary:

Four-billion years of continuous partial melting of Earth's mantle leaves behind the depleted residual mantle. Some residual mantle is isotopically more depleted than mid-ocean ridge basalts, named as ultra-depleted mantle (UDM). UDM is ubiquitous beneath the oceanic crust, and no subcontinental UDM has been found. Subcontinental UDM is likely to occur in areas with vast high radiogenic Nd–Hf magmatic rocks. The Central Asian Orogenic Belt (CAOB) is characterized by huge volumes of Phanerozoic high $_{Nd}(t)$–$_{Hf}(t)$ granitoids, which are believed to represent juvenile continental crust, and have led to the widely-cited conclusion that more than 50 % of the Phanerozoic crust within the CAOB is juvenile. Our newly identified 1.7 Ga diorite intrusions in central CAOB have much higher $_{Nd}(t)$, $_{Hf}(t)$ and ^{18}O values than the MORB, and significant Nd-Hf isotope decoupling, indicating the presence of subcontinental UDM. Partial melting of ancient subcontinental UDM produces mafic crust with ultrahigh $_{Nd}(t)$–$_{Hf}(t)$ values. Reworking of this ancient crust can generate the Phanerozoic "juvenile" crust with high $_{Nd}(t)$–$_{Hf}(t)$ values. Thus, our finding of subcontinental UDM argues that high $_{Nd}(t)$–$_{Hf}(t)$ granitoids could also be products of UDM-derived crust reworking, and do not necessarily represent juvenile crust.

Introduction

Four-billion years of continuous partial melting of Earth's mantle leaves behind the depleted residual mantle (Sivell and McCulloch, 1991; Stracke et al., 2019). Its chemical compositions have been widely studied through mid-ocean ridge basalts (MORB) and are characterized by depleted incompatible elements and high radiogenic hafnium (Hf) and neodymium (Nd) isotopes (Liu et al., 2008; Salters and Dick, 2002). The depleted mantle is heterogeneous (Lambart et al., 2019; Liu et al., 2008). Recent Nd and Hf studies on abyssal peridotites found that the ultra-depleted mantle (UDM), which is isotopically more depleted than MORB, is ubiquitous beneath the oceanic crust (Stracke et al., 2019). UDM has previously been believed too refractory to melt, but recent experiments and the discovery of olivine-hosted melt inclusions with extreme Hf–Nd isotopes indicate that UDM is able to yield melt (Sanfilippo et al., 2019; Stracke et al., 2019). All the reported UDMs occur underneath the oceanic crust (e.g., Byerly and Lassiter, 2014; Sanfilippo et al., 2019; Sobolev and Shimizu, 1993; Stracke et al., 2019). The continental crust constitutes some 40% of the surface area of the Earth (Hawkesworth et al., 2010). Whether UDM is present beneath the continental crust, and the roles of UDM melting in continental crust evolution are still pending questions.

Subcontinental UDM is more likely to occur in areas with vast high radiogenic Nd–Hf magmatic rocks. The Central Asian Orogenic Belt (CAOB), one of the largest accretionary orogens on Earth, has formed through long-lived convergence and interaction among multiple Phanerozoic arc systems (Fig. 1a; Jahn

et al., 2004; Sengör et al., 2018; Xiao et al., 2015). The CAOB preserves large volumes of Phanerozoic granitic intrusions and their volcanic equivalents with high $_{Nd}(t)-_{Hf}(t)$ values. These Phanerozoic high $_{Nd}(t)-_{Hf}(t)$ rocks are believed to represent juvenile continental crust, and have led to the widely-cited conclusion that more than 50 % (even up to 90 %, ca. 3 million km^2) of the Phanerozoic crust within the CAOB is juvenile (Amar-Amgalan et al., 2007; Sengör et al., 2018; Tang et al., 2017; Zhang et al., 2014; Wu et al., 2003). The CAOB includes tens of microcontinents and subduction–accretion complexes (Fig. 1; Xiao et al., 2015; Zhou et al., 2018). However, if ancient UDM existed underneath the microcontinents during the CAOB evolution, these Phanerozoic "juvenile" continental rocks may have been generated by reworking of ancient UDM-derived continental crust. In fact, recent research is challenging the concept that the CAOB is made up largely of juvenile crust (i.e., Kröner et al., 2017; Tang et al., 2017).

Compared to high $_{Nd}(t)-_{Hf}(t)$ Phanerozoic granitoids widely distributed across the CAOB, Precambrian igneous rocks, especially those with ultra-depleted Nd–Hf isotopic signatures, are rarely exposed and have been poorly studied (e.g., Zhou et al., 2018). In this study, we identify two 1.7 Ga diorite intrusions in the central Mongolia microcontinent of the CAOB (Fig. S1; southeast CAOB), and conduct a systematic study of zircon U–Pb dating and Hf–O isotope analyses as well as whole rock element and Nd–Hf–O isotope analyses to investigate the nature of subcontinental UDM and evaluate its potential impact on Phanerozoic crustal evolution in accretionary orogens.

Geological background and sampling

The CAOB, situated between the Siberia and Baltica cratons to the north and the Tarim and North China cratons to the south, covers an immense area of 8,745,000 km^2 from the Urals, through Kazakhstan, NW China, Mongolia, and NE China to the Okhotsk Sea in the Russian Far East, and includes tens of microcontinents and subduction–accretion complexes, like the SW-Pacific accretionary orogen (Fig. 1; Xiao et al., 2015; Zhou et al., 2018). The CAOB has been subdivided into Western, Central and Eastern segments, and these three segments reveal similar detrital zircon age spectra with four peaks at 495 Ma, 780 Ma, 1825 Ma and 2600 Ma, indicating that they share a common evolutionary history (e.g., Zhou et al., 2018).

Our study area is located in the Xing'an-Inner Mongolia accretionary terrane (XIMAT) of the central CAOB (Fig. 1). The XIMAT extends for over 2000 km in the ENE direction, and preserves a wealth of Permian-Triassic geological records of Paleo-Asian Ocean subduction–collision (e.g., Eizenhöfer et al., 2014). The Proterozoic basement of the XIMAT, as represented by the Wulanaobao Group (Pt_2w), is intruded by several diorite plutons with exposure areas of 0.5–1 km^2 (Fig. S1). Sixteen diorite samples are collected, and are identified as diorite and diorite porphyrite subtypes based on detailed petrological observations (Fig.

S2).

Analytical results

Zircon U–Pb dating methods and results are shown in Text S1 and Table S1. Zircon crystals are typical igneous origin with well-defined, broad sector zones (Fig. 1), and high Th/U ratios (Fig. S3). Three diorite samples yield weighted mean $^{207}Pb/^{206}Pb$ ages of 1681 ± 10 Ma, 1704 ± 18 Ma, and 1690 ± 3 Ma (Figs. 1c-e). Three diorite porphyrite samples show weighted mean $^{207}Pb/^{206}Pb$ ages of 1703 ± 9 Ma, 1710 ± 16 Ma, and 1699 ± 3 Ma (Figs. 1f-h). In-situ zircon Lu-Hf and O isotope analyses were conducted on two samples (Table S2). Diorite sample TW2308-3 has $_{Hf}(t)$ = +23.5 – +36.8 and ^{18}O = +9.2‰– +10.7‰ (Figs. 2 and 3). Diorite porphyrite sample TW2309-3 has $_{Hf}(t)$ = +29.0 – +35.7 and ^{18}O = +8.9‰– +12.4‰.

Eight diorite and eight diorite porphyrite samples were selected for whole-rock element and Nd–Hf–O isotope analyses (Tables S3 and S4). The diorite samples show variable calc-alkaline to alkaline major element contents (Fig. S4) and light rare earth element (LREE)–enriched chondrite–normalized REE patterns and negative Nb–Ta–Ti anomalies on the primitive mantle-normalized spider diagram (Fig. S5). They have highly positive $_{Nd}(t)$ and $_{Hf}(t)$ values of +13.9 – +15.1 and +27.8 – +28.5, respectively (Figs. 2 and 3). In comparison, eight diorite porphyrite samples exhibit higher MgO (4.9 – 5.6 wt. %) contents, $Mg^{\#}$ (58 – 61) values and high-Mg geochemical affinities (Fig. S6), and show moderate negative Eu anomalies (Eu*=0.65–0.75) and positive Th and Sr anomalies (Sr*=1.99 – 2.28; Fig. S5). The diorite porphyrites have whole-rock $_{Nd}(t)$ values of +11.2 to +12.3 and $_{Hf}(t)$ values of +23.0 to +25.3 (Fig. 2). The diorites show lower whole-rock ^{18}O values (2.5 – 4.2‰) than those of the diorite porphyrite (6.0 – 6.6‰; Fig. 4).

Both diorite and diorite porphyrite samples show strong correlations of major elements, high field strength elements (HFSEs), REEs, Y, and Th with Zr (Fig. S7), and smooth and coherent patterns of REEs and trace elements, indicating their immobility during post-intrusion alteration. Crustal contamination was negligible as evidenced by (1) no inherited zircons, (2) extremely high $_{Nd}(t)$ – $_{Hf}(t)$ values, and (3) the lack of correlations between Th/Nb and La/Sm, Th/Nb and $_{Nd}(t)$, and MgO and Nb/La. In tectonic discrimination diagrams (Fig. S8), both the diorites and diorite porphyrites plot in continental arc fields. They formed in a continental arc setting.

1.7 Ga subcontinental UDM underneath the microcontinent during CAOB evolution

The most significant feature of our high-$Mg^{\#}$ and normal diorites are their extremely high $_{Nd}(t)$ and $_{Hf}(t)$ values, much higher than the depleted mantle

array (Fig. 3) and other mantle components (enriched mantle (EM), EM , and high mantle (HIMU)). Such ultra-depleted Nd–Hf isotope compositions of the magmatic rocks can be inherited only from UDM, and indicate the existence of UDM during CAOB evolution. Another notable feature of UDM is its strong Nd–Hf isotope decoupling (Sanfilippo et al., 2019). The Nd–Hf isotope decoupling means that the $_{Nd}(t)$ and $_{Hf}(t)$ values plot far from the terrestrial array ($_{Hf}(t) = 1.55 * _{Nd}(t) + 1.21$; Vervoort et al., 2011). The value $\Delta_{Hf}(t)$ was defined to represent the deviation of the $_{Hf}(t)$ value from the terrestrial array ($\Delta_{Hf}(t) = _{Hf}(t) - 1.55 * _{Nd}(t) - 1.21$) (Vervoort et al., 2011). Our diorite samples show $\Delta_{Hf}(t)$ values of +3.9 – +5.7 and +3.2 – +6.0, which are comparable with those reported for UDM (Fig. 5). Different models have been proposed for Nd–Hf isotope decoupling, including (1) marine sediment incorporation into the mantle source, (2) recent metasomatism of an ancient depleted peridotite by MORB-like mantle melt, and (3) mantle-melt interaction between an ascending MORB-like mantle melt and ultra-depleted lithospheric mantle (Bizimis et al., 2004; Sanfilippo et al., 2019; Zhang et al., 2020). Regardless of the origin, Nd–Hf isotope decoupling is an intrinsic feature of UDM, and the more depleted the mantle is, the more pronounced the Nd-Hf isotope decoupling (Sanfilippo et al., 2019). Thus, 1.7 Ga UDM existed beneath the central Mongolia microcontinent of the CAOB.

In comparison with melts derived from oceanic UDM, those derived from subcontinental UDM during CAOB evolution show high SiO_2 contents and variable calc-alkaline to alkaline geochemical compositions (Fig. S4). Due to fluid and/or melt metasomatism and/or physical mixing with crustal material, UDM-derived magma has relative enrichments of LILEs, and less depleted Nd–Hf isotopes with $_{Nd}(t)$ up to 21, and $_{Hf}(t)$ up to +104 for oceanic UDM (Stracke et al., 2011). These geochemical differences indicate distinctive mantle architectures between subcontinental and oceanic UDMs (Fig. 6). Continuous partial melting of asthenospheric mantle produces depleted melt and leaves behind ultra-depleted residual mantle (Sanfilippo et al., 2019; Stracke et al., 2019). Upwelling depleted melt and ultra-depleted residual mantle are then preserved in the lithospheric mantle, forming refractory mantle matrix and depleted mantle pockets, while crustal material recycling adds enriched mantle pockets in the lithospheric mantle (Liu et al., 2008; Sanfilippo et al., 2019). The refractory mantle matrix is the primary component of the lithospheric mantle, and is regarded as ubiquitous UDM (Sanfilippo et al., 2019; Stracke et al., 2019). Variably depleted to enriched mantle pockets are randomly dispersed in the UDM matrix. These geochemical differences between the subcontinental and oceanic UDMs may be induced by the amount of refractory mantle matrix versus pockets. Subcontinental UDM has a higher refractory mantle matrix proportion and lower pockets, especially lower enriched pockets, than oceanic UDM (Fig. 6).

Different from normal depleted mantle derived melts, our diorite samples show negative Nb–Ta–Ti anomalies and enrichments in LILEs (Fig. S5). These arc-like geochemical features may be caused by subduction-related fluid and/or melt metasomatism and subducted sediment involvement. Nd–Hf decoupling in

our samples has been previously interpreted as resulting from marine sediment addition (Chauvel et al., 2008). Marine sediment addition can also explain the high ^{18}O values (+8.9‰–+12.4‰) of our samples. We perform binary mixing calculations using depleted mantle and marine sediment as two end-members, and the diorites plot along the mixing lines (Fig. 4). Thus, the diorites are likely derived from a mixed source between UDM and marine sediment. A significant compositional gap between high-$Mg^{\#}$ and normal diorites, and their different evolutionary trends (Fig. S9) suggest that the high-Mg diorite porphyrites cannot be generated by fractional crystallization of the normal diorites. Their element differences may reflect different degrees of partial melting.

Overestimated Phanerozoic crustal growth in accretionary orogens

The CAOB has been regarded as the most pronounced site of Phanerozoic crustal growth on Earth due to the large volumes of Phanerozoic granitoids with high $_{Nd}(t)$–$_{Hf}(t)$. However, Tang et al. (2017) recently argued against high crustal generation rates and instead suggested that the CAOB underwent Paleozoic (540-270 Ma) crustal growth at rates that, at most, are close to the overall global average rates of crustal generation. Kröner et al. (2017) pointed out that considerable amounts of Precambrian crustal rocks are present beneath the Paleozoic-Cenozoic cover, the extent of which may be larger than previously considered, and proposed that truly juvenile crustal materials accout for approximately 20 % of the CAOB crust. Both studies pose an intriguing question of whether reworking of ancient crustal rocks with ultra-depleted isotopic signatures can produce the high $_{Nd}(t)$–$_{Hf}(t)$ Phanerozoic granitoids, and has played a role during the Phanerozoic accretionary history of the CAOB.

Three phases of Neoarchean-Mesoproterozoic magmatic rocks (i.e., 2.5 Ga, 1.8 Ga and 1.4 Ga) have been identified in the microcontinents within the CAOB (For more details, refer to Text S2; Zhou et al., 2018). Our newly identified 1.7 Ga diorite intrusions represent the fourth phase of Precambrian magmatic activity. Although the CAOB is covered by post-intrusion volcanic and sedimentary sequences, igneous and detrital zircon U–Pb geochronology evidence argues that these 1.7 Ga magmatic rocks are widely distributed throughout the whole CAOB. The igneous geochronological evidence includes the 1.72 Ga komatiite in the Xing'an microcontinent (Hu et al., 2003), 1.7 Ga granitic gneiss in the Erguna microcontinent (Sun et al., 2013), 1.69 Ga monzogranite in the central Mongolia microcontinent (Su et al., 2020), 1.74 Ga andesite–dacite–trachyrhyodacite association in the Angara–Kan microcontinent (Nozhkin et al., 2016), and 1.7 Ga mafic dikes in the Central Tianshan microcontinent (Wang et al., 2017). The 1.7 Ga detrital-zircon age peaks have been identified in the Gudongjing Group and Beishan complex of the Beishan microcontinent (Song et al., 2013; Zheng et al., 2018), the Wenquan Complex of the Yili microcontinent (Liu et al., 2014), and the Kiik Group of the Aktau–Mointy microcontinent

(Kanygina et al., 2021). Therefore, ~1.7 Ga crust rocks are widely distributed in microcontinents within the CAOB.

A large dataset of Nd–Hf isotopes for Phanerozoic granitoids within the CAOB was collected, and their initial values were recalculated to 1.7 Ga (Figs. 2a-c and 3). The recalculated zircon $_{Hf}(t)$ and whole-rock $_{Nd}(t)$ values of the Phanerozoic granitoids within the CAOB are much higher than the depleted mantle array (Fig. 3). A UDM does exist at 1.7 Ga beneath CAOB. We then recalculated the $_{Hf}(t)$ and $_{Nd}(t)$ values of our 1.7 Ga diorites to the crystallization ages of the Phanerozoic granitoids. The results overlap with those of Phanerozoic high $_{Hf}(t)$– $_{Nd}(t)$ granitoids (Fig. 3), indicating that the 1.7 Ga diorites could be the source of the Phanerozoic high $_{Hf}(t)$– $_{Nd}(t)$ granitoids. Thus, remelting of these ~1.7 Ga crust rocks could produce the Phanerozoic high $_{Nd}(t)$– $_{Hf}(t)$ granitoids in the CAOB. The following observations further confirmed this idea.

(1) These "juvenile" Phanerozoic granitoids in the CAOB show zircon two–stage model Hf ages of 1.45–2.0 Ga with a peak at 1.72 Ga (Fig. 2c), which is identical to the 1.7 Ga crystallization age of our newly identified diorite intrusions (Fig. 2c).

(2) The Phanerozoic granitoids have whole-rock Nd–Hf isotopic decoupling features similar to those of our diorite samples (Fig. 5). Both could be interpreted as results of marine sediment incorporation (Yu et al., 2017; Zhang et al., 2020).

(3) Oxygen isotopes are stable, and remain unfractionated in the solid continental crust. Phanerozoic high $_{Nd}(t)$– $_{Hf}(t)$ granitoids in the CAOB have extremely high ^{18}O values similar to those of our diorite samples (Fig. 4), and the oxygen isotope compositions could also be derived from the 1.7 Ga continental crust.

(4) The Harker diagrams show notable correlations for our diorite samples and these "juvenile" Phanerozoic granitoids in CAOB (Fig. S10). These close elemental correlations resulted from different degrees of partial melting of 1.7 Ga continental crust.

Therefore, reworking of ancient continental crust with extremely high $_{Nd}(t)$–$_{Hf}(t)$ values could have generated the high $_{Nd}(t)$– $_{Hf}(t)$ granitoids in the CAOB. During the Nuna/Columbia assembly, which overlaps with the 1.7 Ga timeframe, partial melting of marine-sediment metasomatized UDM produced large volumes of late Paleoproterozoic crust with high $_{Nd}(t)$– $_{Hf}(t)$– ^{18}O values and significant Nd–Hf isotope decoupling within the CAOB. Their subsequent episodic remelting produced the Phanerozoic high $_{Nd}(t)$– $_{Hf}(t)$ granitoids in the CAOB. Some recent studies also suggest that ancient crust reworking has been significant in modern accretionary orogens (including continental and oceanic arc systems). The Andean and Cordillera continental arc systems in the eastern Pacific Ocean developed above thick continental lithosphere, and their formation involved notable continental crust recycling and assimilation (Haschke et al., 2002). The Japanese islands in the western Pacific Ocean, a Japan-type arc and a widely accepted modern juvenile terrane, also consist of ancient continen-

tal crust, and their subduction–accretion complexes are also mainly composed of recycled continental crust (Jahn, 2010; Wang et al., 2020). Even underlying some modern oceanic arcs, old continental crust has been identified, such as the Luzon arc (Shao et al., 2015), the Solomon arc (Tapster et al., 2014), and the Vanuatu arc (Buys et al., 2014). Thus, both continental and oceanic arc systems could have involved ancient continental crust reworking.

Conclusions

Ancient (ca. 1.7 Ga) subcontinental UDM with extremely high $_{Nd}(t)-_{Hf}(t)$ values was identified beneath the CAOB for the first time. Partial melting of late Paleoproterozoic subcontinental UDM produced a widely distributed 1.7 Ga crust with ultrahigh $_{Nd}(t)-_{Hf}(t)$ values, and subsequent episodic remelting of this 1.7 Ga crust generated the Phanerozoic high $_{Nd}(t)-_{Hf}(t)$ granitoids in the CAOB. Accretionary Phanerozoic crustal growth in accretionary orogens may have been overestimated and reworking of UDM-derived ancient crust can also generate Phanerozoic high $_{Nd}(t)-_{Hf}(t)$ continental crust.

Acknowledgments

We would like to thank Yinglei Li and Tingting Zhang for their helps in field work and zircon U-Pb analyses. HCL thanks Science Foundation of China University of Petroleum, Beijing (No. 2462018YJRC030) for financial support. Supplemental information and data repository are available at

http://doi.org/10.5281/zenodo.6680553.

References

Amar-Amgalan, S., Tanaica, R., Kobayashi, K., Nakamura, E., 2007. Phanerozoic crustal growth constrained by zircon U-Pb age and Sr-Nd-Hf isotopic evidence from the granitoid rocks in Mongolia. Geochimica Et Cosmochimica Acta 71 (15), A19-A19.

Bizimis, M., Sen, G., Salters, V.J.M., 2004. Hf-Nd isotope decoupling in the oceanic lithosphere: constraints from spinel peridotites from Oahu, Hawaii. Earth Planet Sc Lett 217, 43-58.

Byerly, B.L., Lassiter, J.C., 2014. Isotopically ultradepleted domains in the convecting upper mantle: Implications for MORB petrogenesis. Geology 42, 203-206.

Buys, J., Spandler, C., Holm, R.J., Richards, S.W., 2014. Remnants of ancient Australia in Vanuatu: Implications for crustal evolution of island arcs and tectonic development of the southwest Pacific. Geology 42(11), 939-942.

Chauvel, C., Lewin, E., Carpentier, M., Arndt, N.T., Marini, J.C., 2008. Role of recycled oceanic basalt and sediment in generating the Hf-Nd mantle array. Nature Geoscience 1, 64-67.

Eiler, J. M., Schiano, P., Kitchen, N., Stolper, E. M., 2000, Oxygen-isotope evidence for recycled crust in the sources of mid-ocean-ridge basalts. Nature 403, 530-534.

Eiler, J. M., Carr, M. J., Reagan, M., Stolper, E., 2005, Oxygen isotope constraints on the sources of Central American arc lavas. Geochemistry Geophysics Geosystems 6, 1-28.

Eizenhöfer, P.R., Zhao, G.C., Zhang, J., Sun, M., 2014. Final closure of the Paleo-Asian Ocean along the Solonker Suture Zone: Constraints from geochronological and geochemical data of Permian volcanic and sedimentary rocks. Tectonics 33 (4), 441-463.

Hawkesworth, C.J., Dhuime, B., Pietranik, A.B., Cawood, P.A., Kemp, A.I.S., Storey, C.D., 2010. The generation and evolution of the continental crust. J Geol Soc London 167, 229-248.

Haschke, M., Siebel, W., Gunther, A., Scheuber, E., 2002. Repeated crustal thickening and recycling during the Andean orogeny in north Chile (21 degrees-26 degrees S): Journal of Geophysical Research-Solid Earth 07, B1.

Hu, D.G., Li, H.W., Liu, X.G., Yu, R.W., 2003. Dating of Sm-Nd Isochron Ages of the Jifeng Komatiites from the Da Hinggan Ling. Acta Geoscientia Sinica 24, 405-408.

Jahn, B.M., 2010. Accretionary Orogen and Evolution of the Japanese Islands-Implications from a Sr-Nd Isotopic Study of the Phanerozoic Granitoids from Sw Japan. American Journal of Science 310 (10), 1210-1249.

Jahn, B. M., Capdevila, R., Liu, D. Y., Vernon, A., Badarch, G., 2004. Sources of Phanerozoic granitoids in the transect Bayanhongor-Ulaan Baatar, Mongolia: geochemical and Nd isotopic evidence, and implications for Phanerozoic crustal growth: Journal of Asian Earth Sciences 23, 629-653.

Kanygina, N.A., Tretyakov, A.A., Degtyarev, K.E., Kovach, V.P., Skuzovatov, S.Y., Pang, K.N., Wang, K.L., Lee, H.Y., 2021. Late Mesoproterozoic-early Neoproterozoic quartzite-schist sequences of the Aktau-Mointy terrane (Central Kazakhstan): Provenance, crustal evolution, and implications for paleotectonic reconstruction. Precambrian Res 354.

Kröner, A., Kovach, V., Alexeiev, D., Wang, K.L., Wong, J., Degtyarev, K., Kozakov, I., 2017. No excessive crustal growth in the Central Asian Orogenic Belt: Further evidence from field relationships and isotopic data. Gondwana Research 50, 135-166.

Lambart, S., Koornneef, J.M., Millet, M.A., Davies, G.R., Cook, M., Lissenberg, C.J., 2019. Highly heterogeneous depleted mantle recorded in the lower oceanic

crust. Nat Geosci 12, 482-486.

Li, W. J., Yin, C. Q., Long, X. P., Zhang, J., Xia, X. P., Wang, L. J., 2017. Paleoproterozoic S-type granites from the Helanshan Complex in Inner Mongolia: Constraints on the provenance and the Paleoproterozoic evolution of the Khondalite Belt, North China Craton. Precambrian Research 299, 195-209.

Liu, C.Z., Snow, J.E., Hellebrand, E., Brügmann, G., Von Der Handt, A., Büchl, A., Hofmann, A.W., 2008. Ancient, highly depleted heterogeneous mantle beneath Gakkel ridge, Arctic ocean. Nature 452, 311–316.

Liu, H.S., Wang, B., Shu, L.S., Jahn, B.M., Iizuka, Y., 2014. Detrital zircon ages of Proterozoic meta-sedimentary rocks and Paleozoic sedimentary cover of the northern Yili Block: Implications for the tectonics of microcontinents in the Central Asian Orogenic Belt. Precambrian Res 252, 209-222.

Luo, Z.W., Xu, B., Shi, G.Z., Zhao, P., Faure, M., Chen, Y., 2016. Solonker ophiolite in Inner Mongolia, China: A late Permian continental margin-type ophiolite. Lithos 261, 72-91.

Nozhkin, A.D., Turkina, O.M., Likhanov, I.I., Dmitrieva, N.V., 2016. Late Paleoproterozoic volcanic associations in the southwestern Siberian craton (Angara-Kan block). Russ Geol Geophys+ 57, 247-264.

Salters, V.J.M., Dick, H.J.B., 2002. Mineralogy of the mid-ocean-ridge basalt source from neodymium isotopic composition of abyssal peridotites. Nature 418, 68-72.

Sanfilippo, A., Salters, V., Tribuzio, R., Zanetti, A., 2019. Role of ancient, ultra-depleted mantle in Mid-Ocean-Ridge magmatism. Earth Planet Sc Lett 511, 89-98.

Sengör, A.M.C., Natal'in, B.A., Sunal, G., van der Voo, R., 2018. The Tectonics of the Altaids: Crustal Growth During the Construction of the Continental Lithosphere of Central Asia Between similar to 750 and similar to 130 Ma Ago. Annual Review of Earth and Planetary Sciences, Vol 46 46, 439-494.

Shao, W. Y., Chung, S. L., Chen, W. S., Lee, H. Y., Xie, L. W., 2015. Old continental zircons from a young oceanic arc, eastern Taiwan: Implications for Luzon subduction initiation and Asian accretionary orogeny: Geology 43, 479-482.

Sivell, W.J., McCulloch, M.T., 1991. Neodymium isotope evidence for ultra-depleted mantle in the early Proterozoic. Nature 354, 384–387.

Stracke, A., Genske, F., Berndt, J., Koornneef, J.M., 2019. Ubiquitous ultra-depleted domains in Earth's mantle. Nat Geosci 12, 851-855.

Stracke, A., Snow, J.E., Hellebrand, E., von der Handt, A., Bourdon, B., Birbaum, K., Gunther, D., 2011. Abyssal peridotite Hf isotopes identify extreme mantle depletion. Earth Planet Sc Lett 308, 359-368.

Sobolev, A.V., Shimizu, N., 1993. Ultra-depleted primary melt included in an olivine from the Mid-Atlantic ridge. Nature 363, 151–154.

Song, D.F., Xiao, W.J., Han, C.M., Tian, Z.H., Wang, Z.M., 2013. Provenance of metasedimentary rocks from the Beishan orogenic collage, southern Altaids: Constraints from detrital zircon U-Pb and Hf isotopic data. Gondwana Res 24, 1127-1151.

Su, M.R., Li, Y.L., Liu, H.C., Shao, Y.X., Zhang, Q., Zhou, F., Cao, L., Sun, J.H., 2020. Paleoproterozoic basement in eastern Central Asia Orogenic Belt: Evidence from granite and sedimentary strata in Sino-Mongolia border area. Geology in China 47, 1186-1203 (in Chinese with English abstract).

Sun, L.X., Ren, B.F., Zhao, F.Q., Ji, S.P., Geng, J.Z., 2013. Late Paleoproterozoic magmatic records in the Eerguna massif: evidences from the zircon U-Pb dating of granitic gneisses. Geology Bulletin of China 32, 41–352 (in Chinese with English abstract).

Tapster, S., Roberts, N. M. W., Petterson, M. G., Saunders, A. D., Naden, J., 2014. From continent to intra-oceanic arc: Zircon xenocrysts record the crustal evolution of the Solomon island arc. Geology 42, 1087-1090.

Tang, G.J., Chung, S.L., Hawkesworth, C.J., Cawood, P.A., Wang, Q., Wyman, D.A., Xu, Y.G., Zhao, Z.H., 2017. Short episodes of crust generation during protracted accretionary processes: Evidence from Central Asian Orogenic Belt, NW China. Earth And Planetary Science Letters 464, 142-154.

Valley, J. W., Lackey, J. S., Cavosie, A. J., Clechenko, C. C., Spicuzza, M. J., Basei, M. A. S., Bindeman, I. N., Ferreira, V. P., Sial, A. N., King, E. M., Peck, W. H., Sinha, A. K., Wei, C. S., 2005. 4.4 billion years of crustal maturation: oxygen isotope ratios of magmatic zircon: Contributions to Mineralogy and Petrology 150, 561-580.

Vervoort, J.D., Plank, T., Prytulak, J., 2011. The Hf-Nd isotopic composition of marine sediments. Geochimica Et Cosmochimica Acta 75 (20), 5903-5926.

Wang, J.Y., Santosh, M., Yang, C.X., Nakagawa, M., Dong, Y.P., 2020. Ancient crustal recycling in modern island arcs: A tale of the world's youngest charnockite from SW Japan. Lithos 354, 105360.

Wang, X.S., Gao, J., Klemd, R., Jiang, T., Li, J.L., Zhang, X., Xue, S.C., 2017. The Central Tianshan Block: A microcontinent with a Neoarchean-Paleoproterozoic basement in the southwestern Central Asian Orogenic Belt. Precambrian Res 295, 130-150.

Wu, F. Y., Jahn, B. M., Wilde, S. A., Lo, C. H., Yui, T. F., Lin, Q., Ge, W. C., and Sun, D. Y., 2003, Highly fractionated I-type granites in NE China (II): isotopic geochemistry and implications for crustal growth in the Phanerozoic. Lithos, 67 (3-4), 191-204

Xiao, W.J., Windley, B.F., Sun, S., Li, J.L., Huang, B.C., Han, C.M., Yuan, C.,

Sun, M., Chen, H.L., 2015. A Tale of Amalgamation of Three Permo-Triassic Collage Systems in Central Asia: Oroclines, Sutures, and Terminal Accretion. Annual Review of Earth and Planetary Sciences, Vol 43 43, 477-507.

Yu, Y., Sun, M., Huang, X.L., Zhao, G.C., Li, P.F., Long, X.P., Cai, K.D., Xia, X.P., 2017. Sr-Nd-Hf-Pb isotopic evidence for modification of the Devonian lithospheric mantle beneath the Chinese Altai. Lithos 284, 207-221.

Zheng, R.G., Li, J.Y., Xiao, W.J., Zhang, J., 2018. Nature and provenance of the Beishan Complex, southernmost Central Asian Orogenic Belt. Int J Earth Sci 107, 729-755.

Zhang, C., Liu, D., Zhang, X., Spencer, C., Tang, M., Zeng, J., Jiang, S., Jolivet, M., and Kong, X., 2020. Hafnium isotopic disequilibrium during sediment melting and assimilation. Geochemical Perspectives Letters, 12: 34-39

Zhang, S.H., Zhao, Y., Ye, H., Liu, J.M., Hu, Z.C., 2014. Origin and evolution of the Bainaimiao arc belt: Implications for crustal growth in the southern Central Asian orogenic belt. Geological Society of America Bulletin 126 (9-10), 1275-1300.

Zhou, J.B., Wilde, S.A., Zhao, G.C., Han, J., 2018. Nature and assembly of microcontinental blocks within the Paleo-Asian Ocean. Earth-Science Reviews 186, 76-93.

Figure Captions

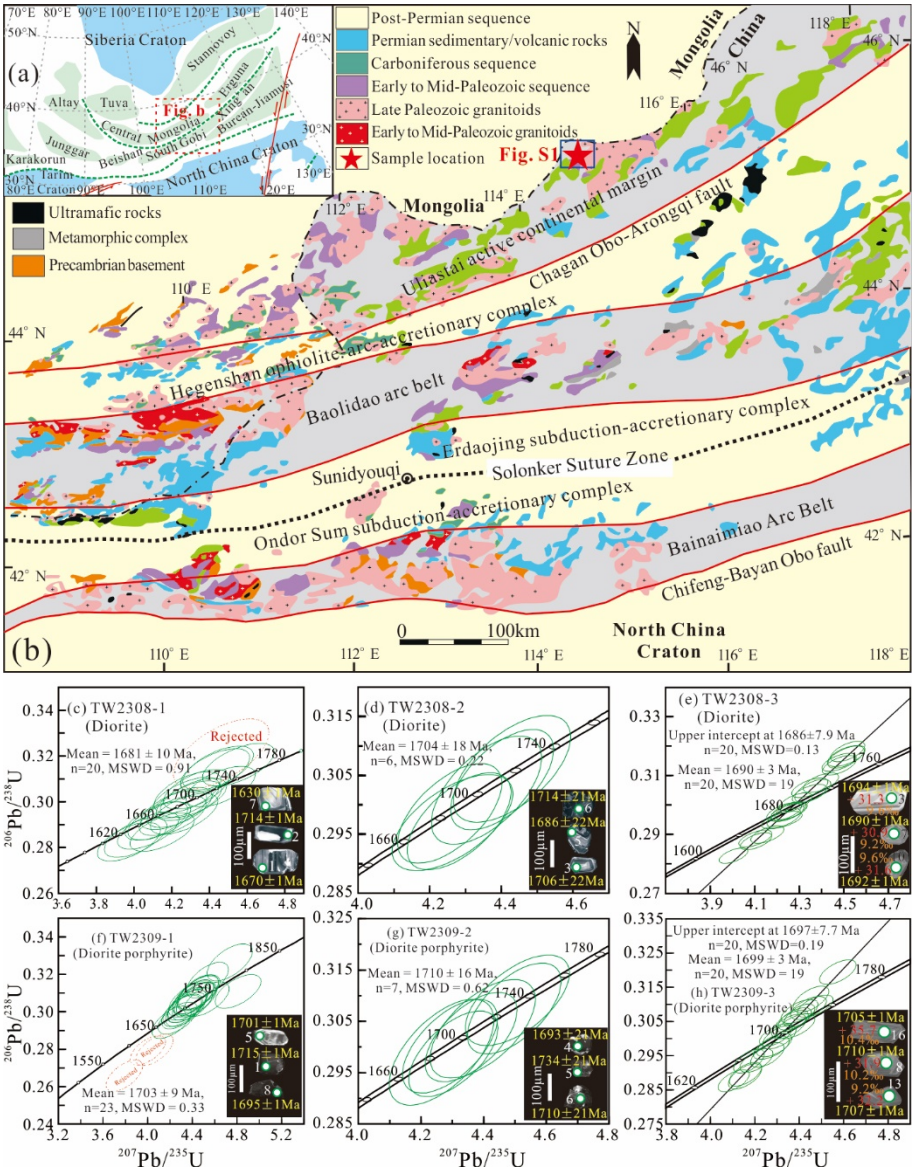

Fig. 1 (a) Simplified geological map showing the cratons and microcontinents within the Paleo-Asian Ocean (Zhou et al., 2018). (b) Geological map of the central Mongolia and South Gobi microcontinents (Wu et al., 2011). (c-h) Laser ablation inductively coupled plasma mass spectrometry (LA–ICP–MS) U–Pb concordia diagrams and cathodoluminescence (CL) images of zircons for the Baoeraobao diorite and diorite porphyrite. Circles on CL images denote the

laser spots.

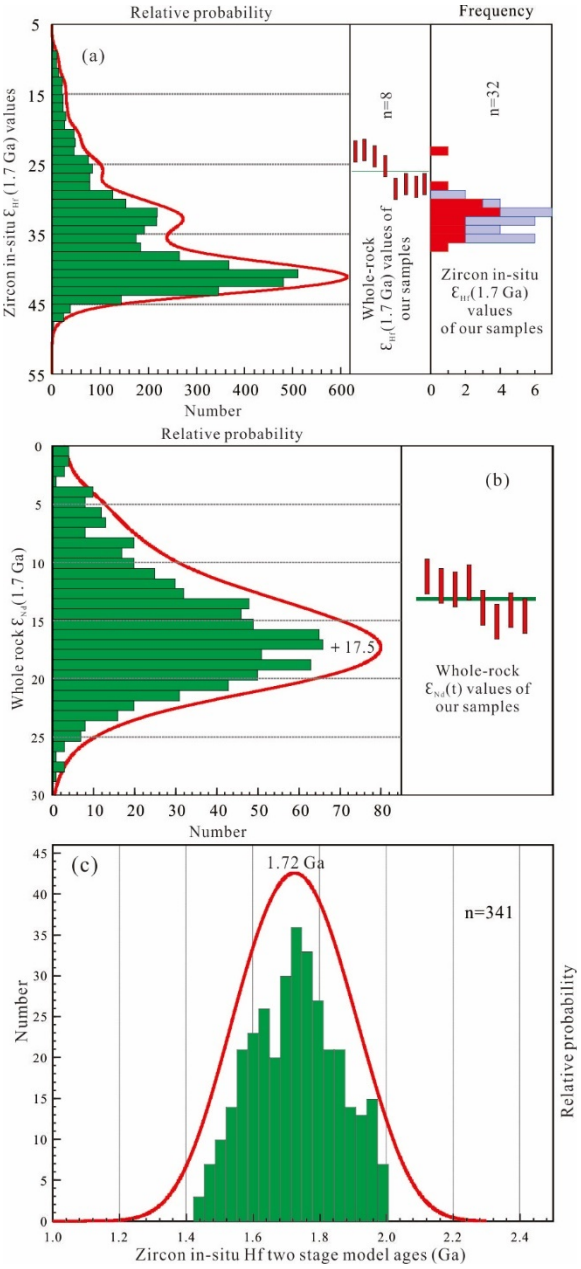

Fig. 2 (a) Relative probability plots of published zircon in-situ $_{Hf}$(t) values of the "juvenile" Phanerozoic granitoids in the CAOB, and whole-rock $_{Hf}$(t) and zircon in-situ $_{Hf}$(t) value plots of our samples. (b) Relative probability plots of published whole-rock $_{Nd}$(t) values of the "juvenile" Phanerozoic granitoids

in the CAOB, and whole-rock $_{Nd}(t)$ value plots of our samples. (c) Relative probability plots of published zircon Hf two-stage model ages of the "juvenile" Phanerozoic granitoids with elevated $_{Nd}(t)$–$_{Hf}(t)$ values in the CAOB. The compiled data are shown in Tables S5 and S6.

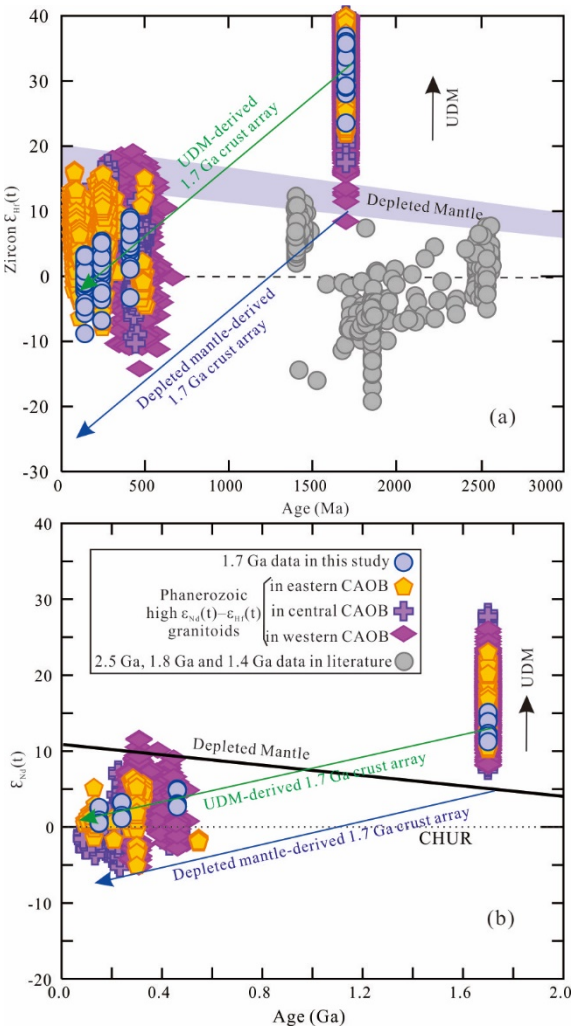

Fig. 3 Age (Ma) versus zircon $_{Hf}(t)$ values (a) and whole-rock $_{Nd}(t)$ values (b). Refs. of the 2.5 Ga, 1.8 Ga and 1.4 Ga data are listed in Text S2. The $_{Hf}(t)$ and $_{Nd}(t)$ values have been recalculated to the crystallization ages of the Phanerozoic granitoids and 1.7 Ga diorites, respectively. The $_{Hf}(t)$ and $_{Nd}(t)$ data, and refs. of the Phanerozoic high $_{Hf}(t)$- $_{Nd}(t)$ granitoids are listed in Tables S5 and S6.

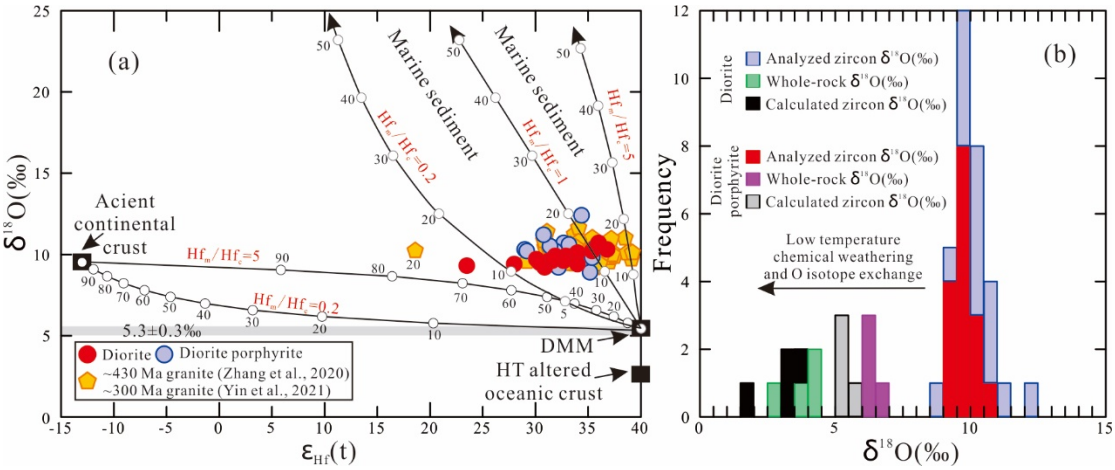

Fig. 4 (a) Plot of zircon $_{Hf}(t)$ versus ^{18}O for our samples. The field for the depleted mantle is represented by the gabbro samples (SGZ-3-1) from the Solonker ophiolite in Inner Mongolia, China from Luo et al. (2016), and its Hf isotope recalculated to 1.7 Ga is $_{Hf}(t) = +40$. The ^{18}O of the depleted MORB mantle (DMM) is set to 5.37‰ according to (Eiler et al., 2000). The field for ancient continental crust is represented by the Paleoproterozoic S-type granites from the Helanshan Complex in Inner Mongolia, China from Li et al. (2017) with $_{Hf}(t) = -13$ and $^{18}O = 9.5‰$. Fields for marine sediments and altered oceanic crust are from Eiler et al. (2005) and Vervoort et al. (2011), with $_{Hf}(t) = +5.5$ and $^{18}O = 41‰$, and $_{Hf}(t) = +40$ and $^{18}O = 2.5‰$, respectively. All $_{Hf}(t)$ values have been recalculated to a crystallization age of 1.7 Ga. (b) Relative probability plots of ^{18}O. Zircon ^{18}O is calculated according to the relation: zircon ^{18}O whole rock $^{18}O - 0.0612*(wt.\% SiO_2) + 2.5$ (Valley et al., 2005).

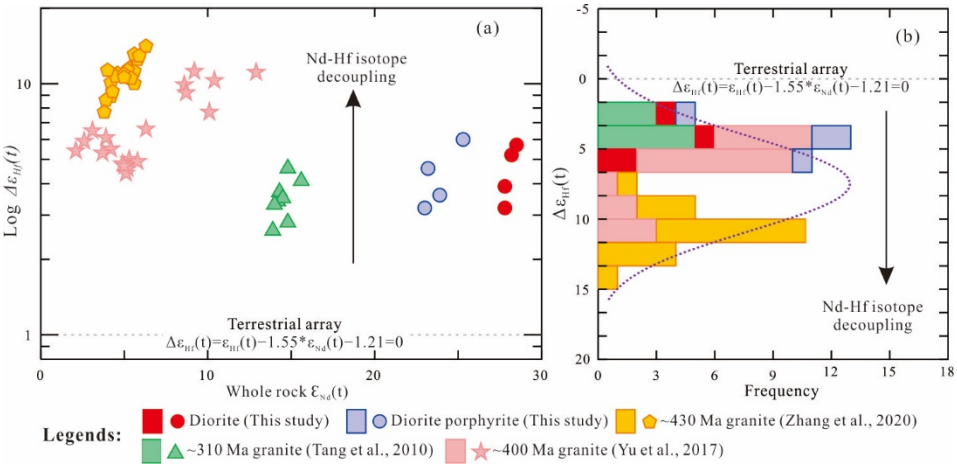

Fig. 5 (a) Whole-rock $_{Nd}(t)$ versus log $\Delta_{Hf}(t)$, and (b) relative probability

plots of $\Delta_{Hf}(t)$. $\Delta_{Hf}(t) = {}_{Hf}(t) - 1.55 * {}_{Nd}(t) - 1.21$.

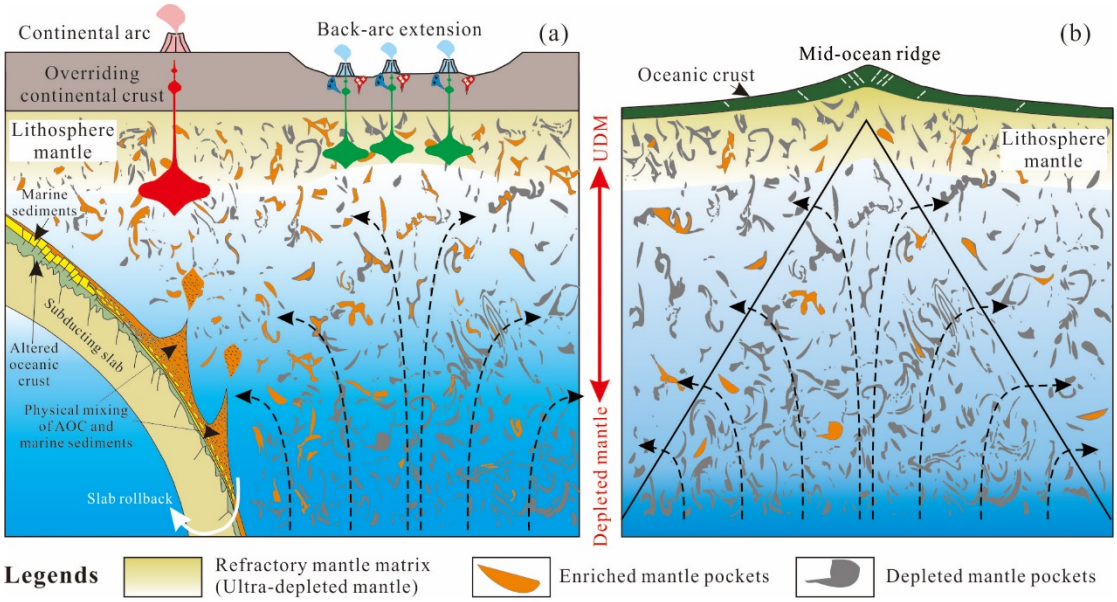

Fig. 6 Schematic cartoons showing different proportions of ancient-refractory mantle matrix containing enriched mantle pockets beneath the oceanic and continental crust (redrawn from Sanfilippo et al., 2019 and Liu et al., 2008).